coatings

MDPI

Article

Sedum Plumbizincicola Derived Functional Carbon for Activation of Peroxymonosulfate to Eliminate Bisphenol A: Performance and Reaction Mechanisms

Chao Liu [1,2,†], Zhenxiang Chen [3,†], Ruiqin Kang [1], Yongsheng Niu [1,*], Wenhui Su [1], Xiaolong Wang [1], Dayong Tian [1] and Ying Xu [2,*]

[1] Department of Environmental Engineering, College of Chemistry and Environmental Engineering, Anyang Institute of Technology, Anyang 455000, China
[2] College of Chemistry and Chemical Engineering, Henan University, Kaifeng 475004, China
[3] Jiangsu Xingzhou Ecological Environment Technology Co., Ltd., Nanjing 210004, China
* Correspondence: nys2205@163.com (Y.N.); hdccxu@126.com (Y.X.)
† These authors contributed equally to this work.

Abstract: Carbon-based functional materials are deemed to be excellent candidates to adsorb contaminants from wastewater, yet their catalytic roles in advanced oxidation processes (AOPs) are still ambiguous. Therefore, four functional carbons (SPFCx) were fabricated in this study under various pyrolysis temperatures by using Sedum plumbizincicola (SP) residues (a kind of phytoremediation plant) as the precursors. Notably, SPFC800 exhibited the best adsorption capacity (q_e = 26.081 mg g^{-1}) toward bisphenol A (BPA) due to its having the largest specific surface area (121.57 m^2 g^{-1}). By injecting peroxymonosulfate (PMS, 5.0 mM), BPA (10 mg L^{-1}) could be completely removed within 70 min. More importantly, the BPA removal was stable and effective even in complex wastewater. Interestingly, radicals played minor roles in the SPFC800/PMS system, while nonradical mechanisms (i.e., $^1O_2$ and electron-transfer regime) were responsible for the BPA elimination, which was verified by quenching tests, solvent exchange experiments ($H_2O_2 \rightarrow D_2O$), and electrochemical experiments. Overall, this work may provide a facile and green method for BPA contaminated-wastewater purification and promote the application of AOPs in environmental remediation.

Keywords: peroxymonosulfate; pre-adsorption; degradation; nonradical oxidation

Citation: Liu, C.; Chen, Z.; Kang, R.; Niu, Y.; Su, W.; Wang, X.; Tian, D.; Xu, Y. Sedum Plumbizincicola Derived Functional Carbon for Activation of Peroxymonosulfate to Eliminate Bisphenol A: Performance and Reaction Mechanisms. *Coatings* **2022**, *12*, 1892. https://doi.org/10.3390/coatings12121892

Academic Editor: Alexandru Enesca

Received: 27 October 2022
Accepted: 28 November 2022
Published: 5 December 2022

1. Introduction

Phytoremediation technology is deemed to be a green environmental protection technology for soil remediation [1–3]. Notably, the core principle of this method is to use hyperaccumulators (e.g., pteris vittata, violabaoshaensis, and ellshohzia splendens) to concentrate the metals from the contaminated soil and then harvest the plants to remove heavy metal pollutants [4,5]. As a result, large amounts of plant-based wastes containing heavy metals are produced during the phytoremediation processes. Notably, these harvests often contain very high concentrations of heavy metals, which may become new sources of pollution upon improper disposal. Therefore, the safe disposal of the harvest is deemed to be an important issue [6,7]. Up until now, several methods (e.g., liquid extraction, landfill, composting treatment, and thermal treatment) have been developed to treat the harvest in the previous studies. Although liquid-phase extraction can effectively extract heavy metals from the plants, the generated extraction liquid needs to be treated, which may cause high treatment costs. In addition, the landfill may take up a lot of land resources, and the ultra-high concentrations of heavy metals in the harvest may migrate into the leachate, which may cause secondary pollution to the soil and groundwater. Therefore, developing an effective, green, and promising technology for the reuse of hyperaccumulator residues is urgent.

Recently, thermal treatment technology has been widely recognized. In particular, thermal treatment can prevent metal leaching, which is conducive to harmless disposal. Notably, value-added functional carbon (FC) can be obtained by pyrolyzing these plant residues under oxygen-limited conditions, which may further be used for water decontamination [8–11]. To our satisfaction, the inherent heavy metals can be converted into metal oxide nanoparticles, which can reduce the release of metallic pollutants [12]. Meanwhile, metal species can tailor the structures of carbon materials [13–16]. Recently, FC has been successfully applied for contaminants degradation in advanced oxidation processes (AOPs) by coupling with various oxidants (e.g., hydrogen peroxide (H_2O_2), periodate (PI), peroxymonosulfate (PMS), and peracetic acid (PAA)) [17–21]. As a result, the specific roles of carbon materials in AOPs were tentatively investigated in previous studies [22–25]. For instance, peroxydisulfate (PDS) could effectively be activated to produce reactive oxygen species (ROS, e.g., $SO_4^{\cdot-}$, $O_2^{\cdot-}$ and $^1O_2$) with the assistance of FC prepared by peanut shells, corn straw, and water hyacinth [26–30]. Despite many attempts, the mechanism of interaction between target pollutants, oxidants, and carbon materials in heterogeneous AOPs remained unclear [31–33].

Due to the large scale of bisphenol A (BPA) utilization, BPA contamination can be found in various environmental compartments (e.g., air, water, and soil), which may cause disease by disrupting the human endocrine system [34]. To this end, several methods (e.g., adsorption, flocculation, and biological treatment) are used for BPA removal [35–38]. Notably, AOPs have been considered as promising methods for BPA elimination in recent years. For example, a series of photocatalysts were designed and applied for the photocatalytic degradation of BPA [34]. However, the constant input of energy may increase the cost of the technology; thus carbon-catalyzed AOPs are deemed to be the promising candidates for pollutants removal.

In this study, Sedum plumbizincicola, which is often used to concentrate heavy metals from contaminated soil, was used for the FC preparation. BPA, which is widely used in the manufacturing industry, was selected as the target pollutant. First, the apparent morphology of the FC was characterized. After that, the adsorptive behaviors of BPA on FC were analyzed by fitting with the kinetic models. Then, the BPA removal was investigated in several AOPs (i.e., FC/PMS, FC/PDS, and FC/H_2O_2 systems). Furthermore, the BPA degradation mechanism was systematically explored by quenching tests, solvent exchange tests, and electrochemical experiments. Additionally, the catalytic activity and stability of the FC were also investigated in real water samples. Overall, this work not only provides a facile and low-cost method for the preparation of functional materials toward environmental remediation but also deepens the understanding of carbon-catalyzed AOPs.

2. Materials and Methods

2.1. Materials

The BPA (≥99%) was purchased from Aladdin. D_2O (99.9%) was purchased from Macklin, Nanjing, China. Quenching agents (e.g., methanol (MeOH, ≥99.9%), L-histidine (*L-his*, 99%), Furfuryl alcohol (FFA, 98%) and *Tert*-butanol (TBA, 99%)) were obtained from Aladdin, Nanjing, China. Other chemicals were at least analytical grade and used without further purification. Ultrapure water (18.25 MΩ) was produced by Spring-S60i + PALL system. In addition, a multifunctional crusher (LINGSUM, 1000C) was used for grinding Sedum plumbizincicola.

2.2. Methods

2.2.1. Preparation and Characterization of FC

Sedum plumbizincicola, a kind of hyperaccumulator collected in Yunnan, China, was used for the FC preparation. Firstly, sedum plumbizincicola was washed with pure water and then dried at 60 °C for 12 h. After that, the dried sedum plumbizincicola was ground to powder, transferred into a crucible, and carbonized in the muffle furnace at the required temperature (i.e., 500 °C, 600 °C, 700 °C, and 800 °C) for 2 h. Then, the black solid block was

ground to desired size by using a 100-mesh sieve, washed with the pure water, and dried at 60 °C (about 4 h) until constant weight. The final products were designated as SPFCx, in which x was the annealing temperature (i.e., 500 °C, 600 °C, 700 °C, and 800 °C). In addition, Field emission scanning electron microscopy (SEM, Fei Quanta 400 FEG, Hillsboro, OR, USA) was used to determine the morphologies of SPFCx. The specific surface area (S_{BET}) was calculated according to the Brunauer-Emmett-Teller equation (Micromeritics ASAP 2020, Micromeritics Instrument Corporation, Norcross, GA, USA).

2.2.2. Adsorption

Adsorption was carried out in several conical flasks (100 mL) that contained 50 mL of BPA solution (10 mg L^{-1}) and 0.2 g L^{-1} of SPFCx. At predetermined time intervals, samples were collected, quenched by MeOH and then analyzed by liquid chromatography. The adsorption behaviors of BPA on SPFCx were determined by kinetic studies. Two kinetic models (i.e., pseudo-first and pseudo-second order kinetic models) were selected to analyze the adsorptive behaviors of BPA on SPFCx:

$$\text{Pseudo first} - \text{order kinetic model} : q_t = q_e\left(1 - e^{-k_1 t}\right) \quad (1)$$

$$\text{Pseudo sec ond} - \text{order kinetic model} : q_t = \frac{k_2 q_e^2 t}{1 + k_2 q_e t} \quad (2)$$

where, q_e and q_t are the adsorption amounts of BPA on SPFCx at equilibrium and time t (mg g^{-1}), respectively. k_1 (min^{-1}) and k_2 (g mg^{-1} min^{-1}) are the corresponding adsorption rate constants, respectively.

2.2.3. Catalytic Degradation of BPA

BPA, an endocrine disruptor, was selected as the target contaminant to assess the catalytic performance of SPFCx. The experiments were conducted as follows: 10 mg SPFCx was first added into the BPA solution (10 mg L^{-1}) and stirred for 40 min to achieve adsorption equilibrium. Then, 5 mM oxidants (e.g., PMS, PDS, and H_2O_2) were injected into the mixture to initiate the catalytic reaction. At predetermined time intervals, 0.5 mL solution was withdrawn, filtered with a 0.2 mm filter to remove the solid catalyst, and quenched with 0.5 mL methanol for analysis.

The elimination of BPA was also tested in real water matrixes (i.e., pure water (PW), river water (RW) from Taihu in Wuxi, chemical wastewater (WW) collected from a sewage treatment plant in Anyang, and tap water (TW)).

2.2.4. Analytical Methods

The concentration of BPA could be detected by Agilent 1260 High Performance Liquid Chromatography (HPLC, Agilent, Beijing, China) equipped with a reversed-phase C18 column (5 μm, 4.6 × 250 mm). The mobile phase contained water and methanol (15/85, v/v). The flow rate was 1.0 mL min^{-1} and the injection volume was 20 μL. Electrochemical experiments were performed on a CHI660E electrochemical workstation and the details of the analytical methods were provided in the Supplementary Materials Text S1. In addition, the $^1O_2$ in SPFC800/PMS systems was identified via electron paramagnetic resonance (EPR, Bruker A320 spectrometer, Bruker, Beijing, China) analysis.

3. Results and Discussion

3.1. Characterizations

In order to evaluate the apparent morphology of the prepared SPFCx, SEM images were conducted. As depicted in Figure 1, the particle size of SPFC500 (Figure 1a) was relatively larger than that of the SPFC800 (Figure 1b), indicating that higher pyrolysis temperature might be beneficial for the complete decomposition of the precursors and the finer particle size may endow SPFC800 with larger S_{BET} and more active sites. It was

reported that higher surface areas and more adsorptive sites were beneficial for removing contaminants [39–42].

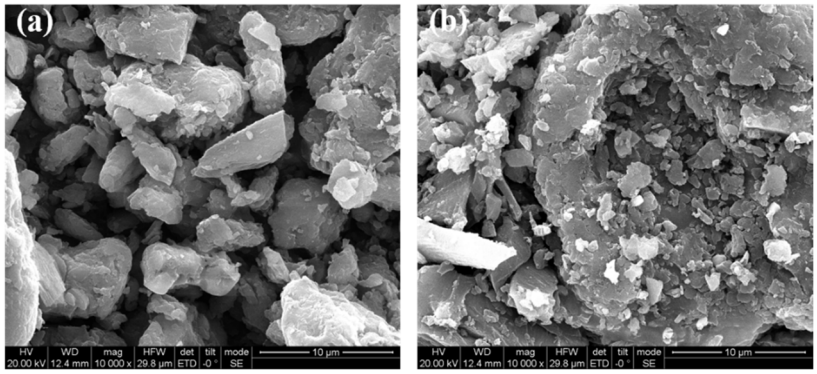

Figure 1. SEM images of SPFC500 (**a**) and SPFC800 (**b**).

In order to further verify the enlargement of surface area with the increasing pyrolysis temperature, the nitrogen adsorption method was carried out to measure the S_{BET} of SPFCx. The structure information of SPFCx was summarized in Table 1. The results demonstrated that with the increase of annealing temperature (from 500 to 800 °C), the S_{BET} significantly increased from 36.09 to 121.57 m^2 g^{-1}, indicating more adsorptive sites were created, which may be beneficial for accumulating the BPA from the solution. The largest S_{BET} of SPFC800 might be owing to the complete decomposition of contents (e.g., fatty acid esters) in precursors. Moreover, the pore volume of SPFCx also increased (from 0.0277 to 0.0847 cm^3 g^{-1}) with increasing pyrolysis temperature, which might be beneficial for producing more active sites. The average pore diameters of SPFCx were between 3.651 and 3.977 nm, suggesting that SPFCx could produce abundant mesoporous pores. Notably, much more meso/micro pores might be formed during higher pyrolysis temperature as evidenced by the smaller pore diameter. The well-interconnected porous structures may contain plenty of nano-spaces/channels, which might be beneficial for the formation of nanoconfinement effects, boosting BPA removal [43,44].

Table 1. The basic information of SPFCx.

Samples	S_{BET} (m^2 g^{-1})	Pore Volume (cm^3 g^{-1})	Average Pore Diameter (nm)
SPFC500	36.09	0.0277	3.997
SPFC600	59.88	0.0592	3.764
SPFC700	78.29	0.0631	3.799
SPFC800	121.57	0.0847	3.651

3.2. Adsorption

As shown in Figure 2a,b, BPA molecule could quickly accumulate on SPFCx surface within 30 min.

Notably, better correlation coefficients (Table 2, R^2 > 0.982) were obtained by fitting with the pseudo-second-order kinetic model, suggesting the adsorption process might be chemisorption. More specifically, SPFC800 exhibited the highest q_e value of 26.081 mg g^{-1}, followed with SPFC700 (21.158 mg g^{-1}), SPFC600 (18.619 mg g^{-1}), and SPFC500 (18.308 mg g^{-1}), indicating the pyrolysis temperature was beneficial for enhancing the adsorption affinity. Thus, it could be speculated that a larger S_{BET} would be obtained under high pyrolysis temperature, which would be beneficial for contaminant adsorption. As depicted in Figure 2c, a good linear relationship between q_e and S_{BET} (R^2 = 0.941) was observed, further confirming that the adsorption of BPA was determined by the specific surface area of SPFCx.

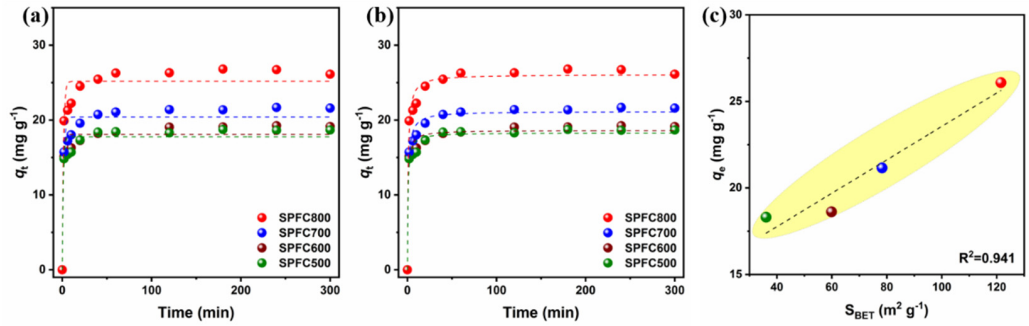

Figure 2. Pseudo first (**a**); pseudo second (**b**) order kinetic models; and the correlation analysis between q_e and S_{BET} (**c**). (Experimental conditions: [BPA] = 10 mg L^{-1}, and [SPFCx] = 0.2 g L^{-1}).

Table 2. The parameters obtained by fitting with adsorption kinetic equation.

Biochar	Pseudo First-Order			Pseudo Second-Order		
	q_e	k_1	R^2	q_e	k_2	R^2
SPFC500	17.771 (0.408)	0.862	0.951	18.308 (0.302)	0.0847	0.982
SPFC600	18.084 (0.411)	0.876	0.951	18.619 (0.307)	0.0855	0.982
SPFC700	20.399 (0.509)	0.674	0.949	21.158 (0.323)	0.0521	0.985
SPFC800	25.184 (0.624)	0.724	0.944	26.081 (0.418)	0.0461	0.983

3.3. Catalytic Degradation Performance

Although H_2O_2 was a traditional and effective oxidant that was usually utilized in Fenton and/or Fenton-Like processes, it could hardly oxidize the BPA even with the help of SPFCx (Figure 3a). The removal of BPA in such an oxidation process was almost attributed to the adsorption by SPFCx. However, a moderate synergistic effect was observed between BPA adsorption and BPA oxidation in SPFCx/PDS systems (Figure 3b). Notably, BPA was more rapidly removed by SPFCx/PMS systems (especially SPFC800), which might be attributed to the non-symmetrical structure of PMS, and thus it was easier to be decomposed (Figure 3c). Due to the highest BPA removal rates in SPFC800/PMS systems, the subsequent BPA degradation experiments would be performed in the SPFC800-induced systems (Figure 3d).

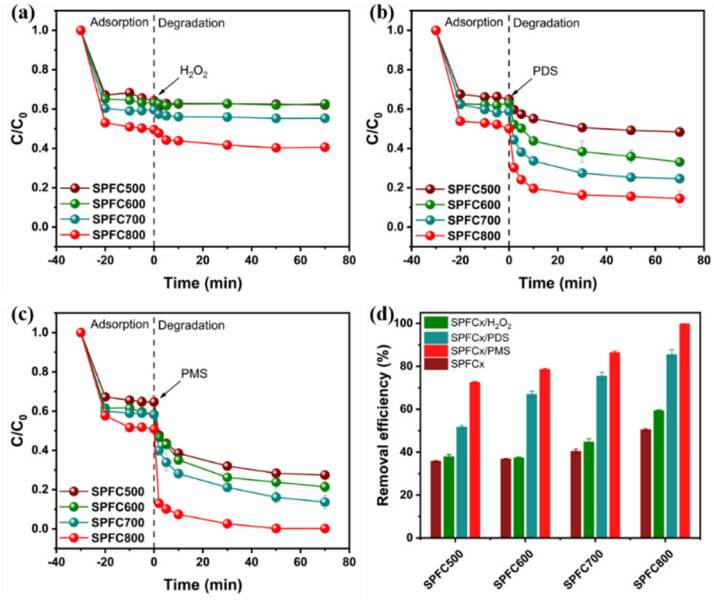

Figure 3. Catalytic degradation of BPA in SPFCx/H_2O_2 (**a**); SPFCx/PDS (**b**); SPFCx/PMS (**c**); systems, respectively, and the removal efficiencies of BPA in various oxidation process (**d**). (Experimental conditions: [BPA] = 10 mg L^{-1}, [Oxidant] = 5 mM, and [SPFCx] = 0.2 g L^{-1}).

3.4. Catalytic Mechanism

In order to reveal why BPA could be quickly and effectively removed in SPCF800/PMS system, quenching experiments were conducted first to demonstrate the involved ROS for BPA removal. Apparently, with the injection of MeOH (Figure 4a, from 500 to 2000 mM), the removal efficiency of BPA was only slightly inhibited, indicating that BPA degradation was not dependent on the radicals (i.e., SO_4^{-} and ·OH). Furthermore, a similar phenomenon was observed by using TBA (quencher for ·OH, from 100 to 1000 mM) as the quenching agent, confirming the minor role of ·OH in BPA elimination (Figure 4b). Nevertheless, both *L-his* and FFA (classic quenchers for $^1O_2$) could significantly inhibit the BPA removal, which suggested that $^1O_2$ might be obligated to the BPA removal (Figure 4c,d). In order to further confirm the existence of $^1O_2$ in SPFC800/PMS system, BPA degradation was conducted in D_2O, which could prolong the half-life of $^1O_2$. As shown in the inset of Figure 4d, BPA removal was boosted in D_2O, demonstrating the vital roles of $^1O_2$ in BPA elimination.

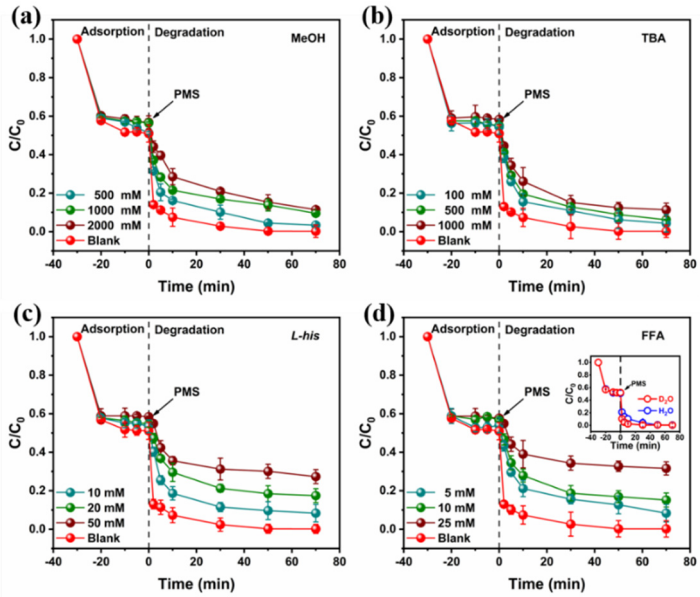

Figure 4. The effects of several quenching agents (i.e., MeOH (**a**); TBA (**b**); *L-his* (**c**); and FFA (**d**)) on BPA removal in SPFC800/PMS system and the solvent exchange experiments (inset of d). (Experimental conditions: [BPA] = 10 mg L^{-1}, [Oxidant] = 5 mM, [SPFCx] = 0.2 g L^{-1}, [MeOH] = 0–2000 mM, [TBA] = 0–1000 mM, [*L-his*] = 0–50 mM, and [FFA] = 0–25 mM).

The EPR test was further conducted to verify the generation of $^1O_2$ in SPFC800/PMS system by using TEMP as the spin-trapping agent (Figure 5). A distinctive triplet signal was detected upon the injection of SPFC800 into the PMS solution, which indicated the existence of $^1O_2$, matching well with the quenching results.

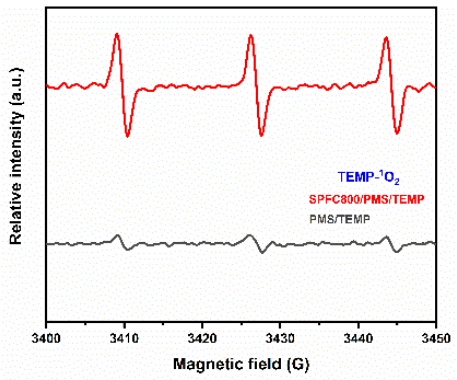

Figure 5. Electron paramagnetic resonance (EPR) spectra of PMS activation by SPFC800: TEMP-$^1O_2$.

In addition, electrochemical experiments were performed to verify the occurrence of electron transfer regime. The EIS results could be used to reveal the resistance of the catalyst. As shown in Figure 6a, SPFC800 possessed a smaller semicircle diameter than SPFC500, indicating the better conductivity of SBC800, and thus electrons could be easier to transfer on SPFC800 surface than SPFC500. The LSV and I-T curves of SPFC800 were also carried out. As shown in Figure 6b, the current density increased upon the injection of PMS, suggesting the rapid interaction between PMS and SPFC800. Furthermore, another obviously increased current density was detected after adding BPA, which might be owing to the electron transfer among BPA (electron donor), PMS (electron acceptor), and SPFC800 (electric conductor). Similarly, as illustrated in Figure 6c, the current responses showed obvious variations upon the injection of PMS and BPA, revealing the vital role of electron transfer mechanism. The potential of the SPFCx surface was characterized to reveal the electron transfer regime in depth. It was well accepted that the PMS could first combine with the catalyst to form the catalyst-PMS complexes (C-PMS*) with higher oxidation capacity. Notably, the C-PMS* was formed first and the potential of C-PMS* significantly increased with the higher dosage of PMS, revealing why BPA generally could be more effectively degraded with higher dosage of oxidants. According to the abovementioned analysis, the reaction mechanism between PMS, BPA, and SPFC800 was elucidated. Nonradicals were the dominant species in the catalytic process, and the SPFC800 could not only directly activate PMS to produce $^1O_2$ but accumulate PMS to form the C-PMS*, leading to effective BPA removal [24,45].

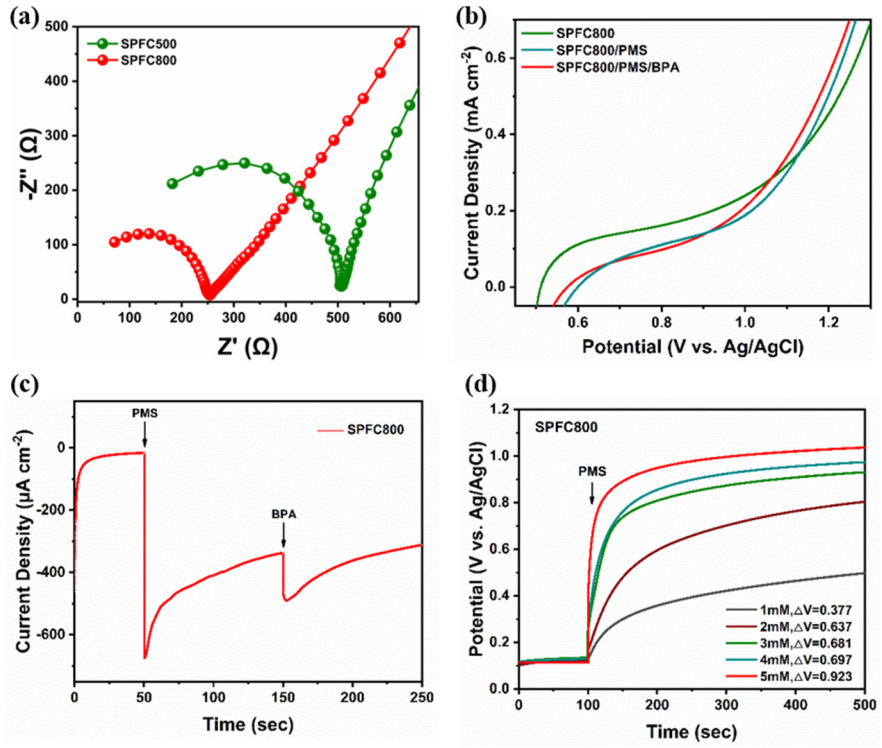

Figure 6. Electrochemical impedance spectroscopy (EIS) of SPFC500 and SPFC800 (**a**); linear sweep voltammetry (LSV) of SPFC800 with/without PMS and BPA (**b**); I-T curves after adding PMS and BPA (**c**); and the change of SPFC800 potential with injection of different concentrations of PMS (**d**).

3.5. Degradation in Real Water

BPA degradation experiments were further conducted in SPFC800/PMS system by adding several interfering substances (i.e., HA, Cl^-, and HCO_3^-). As shown in Figure 7a, the removal of BPA was slightly inhibited by adding 10 mM of HA, which might be owing to that HA could consume PMS and/or the ROS. Similarly, with the injection of HCO_3^-, the BPA degradation was inhibited, which could be due to that the ROS generated in PMS/SPFC800 system were converted into $CO_3^{\bullet-}$ with lower oxidation

capacity (Equations (3) and (4)). Interestingly, BPA removal was slightly accelerated by adding 10 mM of Cl^-, which was attributed to that Cl^- may react with PMS and/or the ROS to form $Cl^•$, synergistically eliminating BPA (Equations (5)–(8)).

$$HO^• + HCO_3^- \rightarrow H_2O + CO_3^{•-} \quad (3)$$

$$SO_4^{-•} + HCO_3^- \rightarrow SO_4^{2-} + HCO_3^- \, , k = 9.1 \times 10^6 \, M^{-1}s^{-1} \quad (4)$$

$$SO_4^{-•} + Cl^- \rightarrow SO_4^{2-} + Cl^• \, , k = 2.0 \times 10^8 \, M^{-1}s^{-1} \quad (5)$$

$$HO^• + Cl^• \rightarrow ClOH^{-•} \quad (6)$$

$$ClOH^{-•} + H^+ \rightarrow Cl^• + H_2O \quad (7)$$

$$Cl^• + Cl^- \rightarrow Cl_2^{-•} \, , \, k = (0.8 - 2.1) \times 10^{10} \, M^{-1}s^{-1} \quad (8)$$

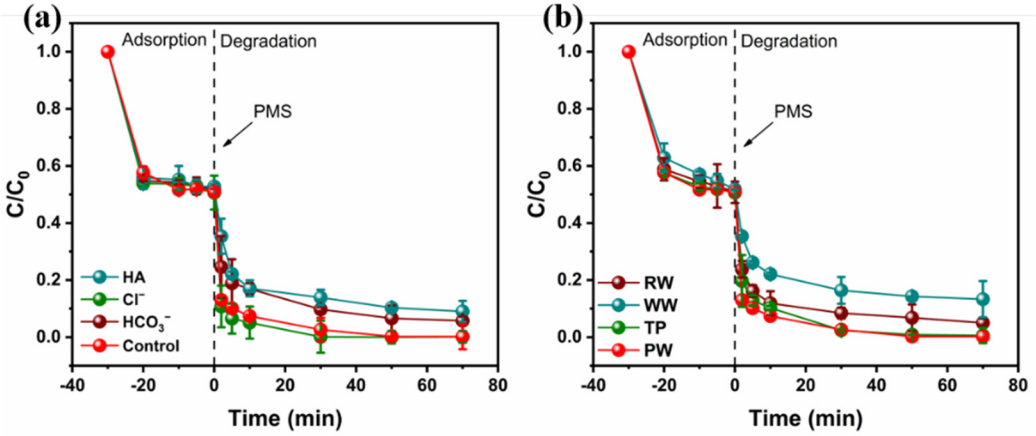

Figure 7. Elimination of BPA in SPFC800/PMS system after adding interfering substances ((**a**), i.e., HA, Cl^-, and HCO_3^-) and degradation of BPA in actual water samples; ((**b**), i.e., RW, WW, TW, and PW). (Experimental conditions: [BPA] = 10 mg L^{-1}, [Oxidant] = 5 mM, [SPFCx] = 0.2 g L^{-1}, [HA] = 5 mg L^{-1}, and [Cl^{-1}] = [HCO_3^-] = 5 mM).

To further evaluate the feasibility of the SPFC800 for BPA elimination, the BPA degradation experiments were carried out in different water matrixes (Table 3). As shown in Figure 7b, BPA removal did not change in TW and was slightly inhibited in RW, which was due to that RW often contained a lot of impurities, consuming the ROS. In addition, a moderate deterioration was observed in WW, which could be owing to the ultra-high concentrations of coexisting contaminants, which could compete with BPA for the ROS.

Table 3. The basic information of the real waters.

Water Sample	pH	COD_{Cr} (mg L^{-1})	Cl^- (mg L^{-1})	NH_4^+-N (mg L^{-1})	PO_4^{3-} (mg L^{-1})
PW	7.2 ± 0.03	<10	0.47	0.09	0.02
TW	7.13 ± 0.03	<10	12.6	1.37	0.138
RW	7.08 ± 0.03	<10	8.52	2.14	0.577
WW	7.44 ± 0.03	572 ± 20	1388	4.11	2.06

4. Conclusions

In this study, a series of sedum plumbizincicola derived functional carbon (SPFCx) catalysts were successfully fabricated. The SPFCx could effectively and rapidly activate PMS for BPA removal. Notably, the catalytic performance was highly decided by the pyrolysis conditions. Among others, SPFC800 exhibited the best catalytic activity because of its highest surface area and pore volumes. In addition, the non-radical pathway (i.e., $^1O_2$ and

electron transfer regime) rather than the radical pathway dominated the BPA degradation. More importantly, the BPA elimination (>80%) was highly stable and effective even in complex wastewater, demonstrating that the SPFC800/PMS system was promising for BPA-contaminated water remediation. Overall, this work may promote the application of AOPs in environmental remediation.

Supplementary Materials: The following supporting information can be downloaded at: https://www.mdpi.com/article/10.3390/coatings12121892/s1, Supporting Information Text S1: Details of electrochemical experiment.

Author Contributions: C.L.: writing—original draft, formal analysis, investigation, and visualization. Z.C.: writing—original draft, formal analysis, investigation, and supervision. R.K.: writing—reviewing and editing, investigation. Y.N.: writing—reviewing and editing, investigation. W.S.: writing—reviewing and editing, investigation. X.W.: writing—reviewing and editing, investigation. D.T.: conceptualization, methodology. Y.X.: formal analysis, resources, writing—review and editing. All authors have read and agreed to the published version of the manuscript.

Funding: This work has been supported by the Research Project of Science and Technology of the Anyang City (2022C01NY016), the Research Project of Science and Technology of the Henan Province (222102320274), PhD research startup foundation of Anyang Institute of Technology (BSJ2021035), Postdoc research startup foundation of Anyang Institute of Technology (BHJ2022005), Postdoc research startup foundation of the Henan Province (202103099), and Major science and technology projects of Anyang (201928).

Institutional Review Board Statement: This article does not contain any studies with human participants or animals performed by any of the authors.

Informed Consent Statement: Not applicable.

Data Availability Statement: Not applicable.

Conflicts of Interest: The authors declare no conflict of interest.

References

1. Oladoye, P.O.; Olowe, O.M.; Asemoloye, M.D. Phytoremediation technology and food security impacts of heavy metal contaminated soils: A review of literature. *Chemosphere* **2022**, *288*, 132555. [CrossRef]
2. Yin, Z.; Yu, J.; Han, X.; Wang, H.; Yang, Q.; Pan, H.; Lou, Y.; Zhuge, Y. A novel phytoremediation technology for polluted cadmium soil: Salix integra treated with spermidine and activated carbon. *Chemosphere* **2022**, *306*, 135582. [CrossRef]
3. Sarma, H.; Islam, N.F.; Prasad, R.; Prasad, M.N.V.; Ma, L.Q.; Rinklebe, J. Enhancing phytoremediation of hazardous metal(loid)s using genome engineering CRISPR-Cas9 technology. *J. Hazard. Mater.* **2021**, *414*, 125493. [CrossRef]
4. Fadhile Almansoory, A.; Abu Hasan, H.; Idris, M.; Sheikh Abdullah, S.R.; Anuar, N. Potential application of a biosurfactant in phytoremediation technology for treatment of gasoline-contaminated soil. *Ecol. Eng.* **2015**, *84*, 113–120. [CrossRef]
5. Zhang, J.; Cao, X.; Yao, Z.; Lin, Q.; Yan, B.; Cui, X.; He, Z.; Yang, X.; Wang, C.H.; Chen, G. Phytoremediation of Cd-contaminated farmland soil via various Sedum alfredii-oilseed rape cropping systems: Efficiency comparison and cost-benefit analysis. *J. Hazard. Mater.* **2021**, *419*, 126489. [CrossRef]
6. Cui, X.; Zhang, J.; Wang, X.; Pan, M.; Lin, Q.; Khan, K.Y.; Yan, B.; Li, T.; He, Z.; Yang, X.; et al. A review on the thermal treatment of heavy metal hyperaccumulator: Fates of heavy metals and generation of products. *J. Hazard. Mater.* **2021**, *405*, 123832. [CrossRef]
7. Guo, X.; Zhang, S.; Luo, J.; Pan, M.; Du, Y.; Liang, Y.; Li, T. Integrated glycolysis and pyrolysis process for multiple utilization and cadmium collection of hyperaccumulator Sedum alfredii. *J. Hazard. Mater.* **2022**, *422*, 126859. [CrossRef]
8. Huo, X.; Zhou, P.; Zhang, J.; Liu, Y.; Cheng, X.; Liu, Y.; Li, W.; Zhang, Y. N, S-Doped porous carbons for persulfate activation to remove tetracycline: Nonradical mechanism. *J. Hazard. Mater.* **2020**, *391*, 122055. [CrossRef]
9. Pei, X.; Peng, X.; Jia, X.; Wong, P.K. N-doped biochar from sewage sludge for catalytic peroxydisulfate activation toward sulfadiazine: Efficiency, mechanism, and stability. *J. Hazard. Mater.* **2021**, *419*, 126446. [CrossRef]
10. Xiao, P.; Yi, X.; Wu, M.; Wang, X.; Zhu, S.; Gao, B.; Liu, Y.; Zhou, H. Catalytic performance and periodate activation mechanism of anaerobic sewage sludge-derived biochar. *J. Hazard. Mater.* **2021**, *424*, 127692. [CrossRef]
11. Yu, J.; Feng, H.; Tang, L.; Pang, Y.; Zeng, G.; Lu, Y.; Dong, H.; Wang, J.; Liu, Y.; Feng, C.; et al. Metal-free carbon materials for persulfate-based advanced oxidation process: Microstructure, property and tailoring. *Prog. Mater. Sci.* **2020**, *111*, 100654. [CrossRef]
12. Yao, Y.; Gao, B.; Chen, J.; Yang, L. Engineered biochar reclaiming phosphate from aqueous solutions: Mechanisms and potential application as a slow-release fertilizer. *Environ. Sci. Technol.* **2013**, *47*, 8700–8708. [CrossRef] [PubMed]

13. Xiao, X.; Chen, B.; Chen, Z.; Zhu, L.; Schnoor, J.L. Insight into Multiple and Multilevel Structures of Biochars and Their Potential Environmental Applications: A Critical Review. *Environ. Sci. Technol.* **2018**, *52*, 5027–5047. [CrossRef] [PubMed]
14. Yao, B.; Luo, Z.; Du, S.; Yang, J.; Zhi, D.; Zhou, Y. Magnetic MgFe2O4/biochar derived from pomelo peel as a persulfate activator for levofloxacin degradation: Effects and mechanistic consideration. *Bioresour. Technol.* **2022**, *346*, 126547. [CrossRef] [PubMed]
15. Liu, J.; Liu, H.; Yang, X.; Jia, X.; Cai, M.; Bao, Y. Preparation of Si-Mn/biochar composite and discussions about characterizations, advances in application and adsorption mechanisms. *Chemosphere* **2021**, *281*, 130946. [CrossRef]
16. Long, Y.; Dai, J.; Zhao, S.; Huang, S.; Zhang, Z. Metal-organic framework-derived magnetic carbon for efficient decontamination of organic pollutants via periodate activation: Surface atomic structure and mechanistic considerations. *J. Hazard. Mater.* **2021**, *424*, 126786. [CrossRef]
17. Zhang, X.; Miao, X.; Xiang, W.; Zhang, J.; Cao, C.; Wang, H.; Hu, X.; Gao, B. Ball milling biochar with ammonia hydroxide or hydrogen peroxide enhances its adsorption of phenyl volatile organic compounds (VOCs). *J. Hazard. Mater.* **2021**, *403*, 123540. [CrossRef]
18. Hassan, M.F.; Sabri, M.A.; Fazal, H.; Hafeez, A.; Shezad, N.; Hussain, M. Recent trends in activated carbon fibers production from various precursors and applications—A comparative review. *J. Anal. Appl. Pyrolysis* **2020**, *145*, 104715. [CrossRef]
19. Wang, X.; Liu, Y.; Zhu, L.; Li, Y.; Wang, K.; Qiu, K.; Tippayawong, N.; Aggarangsi, P.; Reubroycharoen, P.; Wang, S. Biomass derived N-doped biochar as efficient catalyst supports for CO_2 methanation. *J. CO2 Util.* **2019**, *34*, 733–741. [CrossRef]
20. Feng, D.; Lü, J.; Guo, S.; Li, J. Biochar enhanced the degradation of organic pollutants through a Fenton process using trace aqueous iron. *J. Environ. Chem. Eng.* **2021**, *9*, 104677. [CrossRef]
21. Anfar, Z.; Ait El Fakir, A.; Ait Ahsaine, H.; Zbair, M.; Farsad, S.; Morlet-Savary, F.; Jada, A.; El Alem, N. Nitrogen doped graphitic porous carbon from almond shells as an efficient persulfate activator for organic compound degradation. *New J. Chem.* **2020**, *44*, 9391–9401. [CrossRef]
22. Dou, J.; Cheng, J.; Lu, Z.; Tian, Z.; Xu, J.; He, Y. Biochar co-doped with nitrogen and boron switching the free radical based peroxydisulfate activation into the electron-transfer dominated nonradical process. *Appl. Catal. B Environ.* **2022**, *301*, 120832. [CrossRef]
23. He, L.; Yang, C.; Ding, J.; Lu, M.-Y.; Chen, C.-X.; Wang, G.-Y.; Jiang, J.-Q.; Ding, L.; Liu, G.-S.; Ren, N.-Q.; et al. Fe, N-doped carbonaceous catalyst activating periodate for micropollutant removal: Significant role of electron transfer. *Appl. Catal. B Environ.* **2022**, *303*, 120880. [CrossRef]
24. Wang, H.; Guo, W.; Liu, B.; Si, Q.; Luo, H.; Zhao, Q.; Ren, N. Sludge-derived biochar as efficient persulfate activators: Sulfurization-induced electronic structure modulation and disparate nonradical mechanisms. *Appl. Catal. B Environ.* **2020**, *279*, 119361. [CrossRef]
25. Xiong, W.; Wang, Z.; He, S.; Hao, F.; Yang, Y.; Lv, Y.; Zhang, W.; Liu, P.; Luo, H.a. Nitrogen-doped carbon nanotubes as a highly active metal-free catalyst for nitrobenzene hydrogenation. *Appl. Catal. B Environ.* **2020**, *260*, 118105. [CrossRef]
26. Feng, Z.; Zhou, B.; Yuan, R.; Li, H.; He, P.; Wang, F.; Chen, Z.; Chen, H. Biochar derived from different crop straws as persulfate activator for the degradation of sulfadiazine: Influence of biomass types and systemic cause analysis. *Chem. Eng. J.* **2022**, *440*, 135669. [CrossRef]
27. Lian, F.; Cui, G.; Liu, Z.; Duo, L.; Zhang, G.; Xing, B. One-step synthesis of a novel N-doped microporous biochar derived from crop straws with high dye adsorption capacity. *J. Environ. Manag.* **2016**, *176*, 61–68. [CrossRef]
28. Wang, Y.P.; Liu, Y.L.; Tian, S.Q.; Yang, J.J.; Wang, L.; Ma, J. Straw biochar enhanced removal of heavy metal by ferrate. *J. Hazard. Mater.* **2021**, *416*, 126128. [CrossRef]
29. Wang, H.; Xu, J.; Sheng, L. Preparation of straw biochar and application of constructed wetland in China: A review. *J. Clean. Prod.* **2020**, *273*, 123131. [CrossRef]
30. Duan, R.; Ma, S.; Xu, S.; Wang, B.; He, M.; Li, G.; Fu, H.; Zhao, P. Soybean straw biochar activating peroxydisulfate to simultaneously eliminate tetracycline and tetracycline resistance bacteria: Insights on the mechanism. *Water Res* **2022**, *218*, 118489. [CrossRef] [PubMed]
31. Miao, J.; Geng, W.; Alvarez, P.J.J.; Long, M. 2D N-Doped Porous Carbon Derived from Polydopamine-Coated Graphitic Carbon Nitride for Efficient Nonradical Activation of Peroxymonosulfate. *Environ. Sci. Technol.* **2020**, *54*, 8473–8481. [CrossRef]
32. Minakata, D.; Kamath, D.; Maetzold, S. Mechanistic Insight into the Reactivity of Chlorine-Derived Radicals in the Aqueous-Phase UV-Chlorine Advanced Oxidation Process: Quantum Mechanical Calculations. *Environ. Sci. Technol.* **2017**, *51*, 6918–6926. [CrossRef] [PubMed]
33. Peng, J.; Zhou, P.; Zhou, H.; Liu, W.; Zhang, H.; Zhou, C.; Lai, L.; Ao, Z.; Su, S.; Lai, B. Insights into the Electron-Transfer Mechanism of Permanganate Activation by Graphite for Enhanced Oxidation of Sulfamethoxazole. *Environ. Sci. Technol.* **2021**, *55*, 9189–9198. [CrossRef] [PubMed]
34. Reddy, P.V.L.; Kim, K.H.; Kavitha, B.; Kumar, V.; Raza, N.; Kalagara, S. Photocatalytic degradation of bisphenol A in aqueous media: A review. *J. Environ. Manag.* **2018**, *213*, 189–205. [CrossRef]
35. Moradi, F.G.M. Application of peroxymonosulfate and its activation methods for degradation of environmental organic pollutants: Review. *Chem. Eng. J.* **2017**, *310*, 41–62. [CrossRef]
36. Lu, C.S.; Tsai, H.Y.; Shaya, J.; Golovko, V.B.; Wang, S.Y.; Liu, W.J.; Chen, C.C. Degradation of sulfamethoxazole in water by AgNbO3 photocatalyst mediated by persulfate. *RSC Adv.* **2022**, *12*, 29709–29718. [CrossRef]

37. Zhang, Y.; Cui, W.; An, W.; Liu, L.; Liang, Y.; Zhu, Y. Combination of photoelectrocatalysis and adsorption for removal of bisphenol A over TiO2-graphene hydrogel with 3D network structure. *Appl. Catal. B Environ.* **2018**, *221*, 36–46. [CrossRef]
38. Wang, K.; Qiu, L.; Zhu, J.; Sun, Q.; Qu, W.; Yu, Y.; Zhao, Z.; Yu, Y.; Shao, G. Environmental contaminant BPA causes intestinal damage by disrupting cellular repair and injury homeostasis in vivo and in vitro. *Biomed. Pharm.* **2021**, *137*, 111270. [CrossRef] [PubMed]
39. Huang, D.; Zhang, Q.; Zhang, C.; Wang, R.; Deng, R.; Luo, H.; Li, T.; Li, J.; Chen, S.; Liu, C. Mn doped magnetic biochar as persulfate activator for the degradation of tetracycline. *Chem. Eng. J.* **2020**, *391*, 123532. [CrossRef]
40. Liu, B.; Guo, W.; Wang, H.; Si, Q.; Zhao, Q.; Luo, H.; Ren, N. B-doped graphitic porous biochar with enhanced surface affinity and electron transfer for efficient peroxydisulfate activation. *Chem. Eng. J.* **2020**, *396*, 125119. [CrossRef]
41. Qu, S.; Yuan, Y.; Yang, X.; Xu, H.; Mohamed, A.K.; Zhang, J.; Zhao, C.; Liu, L.; Wang, B.; Wang, X.; et al. Carbon defects in biochar facilitated nitrogen doping: The significant role of pyridinic nitrogen in peroxymonosulfate activation and ciprofloxacin degradation. *Chem. Eng. J.* **2022**, *441*, 135864. [CrossRef]
42. Zhu, K.; Wang, X.; Chen, D.; Ren, W.; Lin, H.; Zhang, H. Wood-based biochar as an excellent activator of peroxydisulfate for Acid Orange 7 decolorization. *Chemosphere* **2019**, *231*, 32–40. [CrossRef] [PubMed]
43. Qian, J.; Gao, X.; Pan, B. Nanoconfinement-Mediated Water Treatment: From Fundamental to Application. *Environ. Sci. Technol.* **2020**, *54*, 8509–8526. [CrossRef] [PubMed]
44. Teng, Y.; Liu, E.; Ding, R.; Liu, K.; Liu, R.; Wang, L.; Yang, Z.; Jiang, H. Bean dregs-based activated carbon/copper ion supercapacitors. *Electrochim. Acta* **2016**, *194*, 394–404. [CrossRef]
45. Chen, Y.-d.; Duan, X.; Zhang, C.; Wang, S.; Ren, N.-Q.; Ho, S.-H. Graphitic biochar catalysts from anaerobic digestion sludge for nonradical degradation of micropollutants and disinfection. *Chem. Eng. J.* **2020**, *384*, 123244. [CrossRef]